TIME-FREQUENCY ANALYSIS OF SEISMIC DATA FOR THE CHARACTERIZATION OF GEOLOGIC STRUCTURES VIA SYNCHROEXTRACTING TRANSFORM

ZHEN LI[1,2], JINGHUAI GAO[1,2], ZHIGUO WANG[2,3], NAIHAO LIU[1,2] and FENGYUAN SUN[1,2]

[1] School of Information and Communications Engineering, Xi'an Jiaotong University, Xi'an, Shaanxi 710049, P.R. China. lijiasanshao@stu.xjtu.edu.cn; naihao_liu@mail.xjtu.edu.cn; kerwinsun1@stu.xjtu.edu.cn
[2] National Engineering Laboratory for Offshore Oil Exploration, Xi'an, Shaanxi 710049, P.R. China.
[3] School of Mathematics and Statistics, Xi'an Jiaotong University, Xi'an, Shaanxi 710049, P.R. China. jhgao@mail.xjtu.edu.cn.

(Received December 3, 2018; revised version accepted November 10, 2020)

ABSTRACT

Li, Z., Gao, J.H., Wang, Z.G., Liu, N.H. and Sun, F.Y., 2020. Time-frequency analysis of seismic data for the characterization of geologic structures via synchroextracting transform. *Journal of Seismic Exploration*, 30: 101-120.

Time-frequency (TF) analysis based method is one of the most powerful tools in seismic data processing and interpretation. To delineate the subsurface geological structures clearly, the energy concentration of the seismic TF representation (TFR) is as high as possible. The traditional TF methods, such as the short-time Fourier transform (STFT) and wavelet transform (WT), have been widely applied for seismic TF analysis. However, they suffer from the diffused TFR because of the Heisenberg uncertainty principle. To achieve a higher energy-concentrated TF result, the synchrosqueezing transform (SST) was proposed. The SST method has been successfully used for seismic processing. In this paper, we introduce a novel approach for seismic spectrum analysis based on the synchroextracting transform (SET), which is an extension of the Fourier-based SST (FSST). The SET extracts the TF information only located at the instantaneous frequency (IF) trajectory of the analyzed signal and removes the most smeared TF energy, which leads to a highly sharpened TFR. We also put forward a theorem to prove that the SET can get the exact IF of a linear chirp signal. All the results of the synthetic signal and real seismic data demonstrate the validity and effectiveness of the proposed method.

KEY WORDS: time-frequency analysis, seismic data processing, high energy-concentrated, synchroextracting transform, Fourier-based synchrosqueezing transform.

0963-0651/21/$5.00

INTRODUCTION

Time-frequency analysis (TFA) is a significant tool to process and interpret non-stationary seismic signals to discover the available information. The TFA method transforms a 1D signal into a 2D time-frequency plane, which is widely applied to characterize time-varying features of the seismic data. The linear TFA technique is one important type of the most traditional TFA methods.

The short-time Fourier transform (STFT), wavelet transform (WT), and S-transform (ST) are three representative linear TFA methods. Since 1999, the STFT has been successfully used to process the field seismic data (Partyka and Gridley, 1999; Lu and Zhang, 2009). However, the predefined window length of the STFT provides an invariable spectral resolution (Mallat, 2008; Lu and Li, 2013). In practice, the long window length can provide a high-frequency resolution but a low time resolution. Conversely, a short window length provides a high time resolution but a low-frequency resolution (Tary et al., 2014). The fixed time-frequency (TF) resolution limits the seismic application of the STFT. As an improvement to enhance the property interpretation of a seismic signal, the WT overcomes the drawback of the STFT with a certain extent and offers a superior variable spectral resolution (Morlet et al., 1982; Daubechies, 1992). The WT is one of the most widely used TFA methods. New wavelet basis functions are still proposed to enhance the adaptation for the seismic signal processing (Gao et al., 2006; Lilly and Olhede, 2010; Wang et al., 2017). However, the choice of parameters that makes the wavelet basis function best matching the given signal is a problem (Daubechies, 1992; Gao et al., 1996). Stockwell et al. (1996) proposed the ST, which inherits the advantages of the STFT and WT. However, the resolution is dependent on the frequency, which limits the flexibility of its ST. Several variations of the ST have been proposed and successfully applied in seismic data processing and interpretation (Gao et al., 2003; Sejdić et al., 2008; Liu et al., 2018). Unfortunately, these linear TF approaches are all restricted by the Heisenberg uncertainty principle, which denotes that the best time and frequency resolutions cannot be attained simultaneously (Gabor, 1946; Hlawatesch and Boudreaux, 1992). Thus, the time-frequency representation (TFR) obtained by these classical linear methods are always diffused near the center frequency of a signal.

In seismic data processing, the blurry TFR will be bad for the subsequent geological interpretation, such as the channel detection and hydrocarbon indicator (Li et al., 2016; Liu et al., 2018). To improve the readability or quality of the TFR, some advanced approaches have been proposed including the matching pursuit (MP) algorithms (Mallat and Zhang, 1993; Liu and Marfurt, 2007), the reassignment methods (RM) (Auger and Flandrin, 1995; Auger et al., 2013) and the synchrosqueezing transform (SST) (Daubechies and Maes, 1996; Daubechies et al., 2011). The MP is an adaptive method and can get a sparse TFR. It has been applied for field seismic spectrum analysis (Wang, 2007; Wang et al. 2016). Nevertheless, the time cost of the MP is slightly expensive, especially for the big storage of the 3D seismic volume. The RM reassigns the TF

coefficients into the instantaneous frequency (IF) trajectory. Thus, the RM obtains a high concentrated TFR. However, it is unable to reconstruct the original signal because of the insufficient TF information. As a special case of the RM, the SST only squeezes the TF coefficients along the IF in the frequency direction to enhance the concentration of the TFR. The SST allows for the signal reconstruction but suffers from a lower TF concentration for the strong frequency-modulated (FM) signal (Daubechies et al., 2011). Even so, the SST has been widely applied in seismic data processing (Chen et al., 2014; Herrera et al., 2014; Wang et al., 2014; Liu et al., 2016; Liu et al., 2017). Based on the SST algorithm, several extensions of the SST have been proposed recently and applied in seismic data application, for example, the synchrosqueezed wave packet transform (Wang and Gao, 2017), STFT-based SST (FSST) (Oberlin, 2014), synchrosqueezing three parameter wavelet transform (SST-TPW) (Liu et al., 2015) and synchrosqueezing generalized S-Transform (SSGST) (Wang et al., 2018). As is well known, these SST-based methods are suitable for signals with slowly varying IF, and it will suffer from the blurred TFR for the signals with fast varying IF (Daubechies et al., 2011; Li and Liang, 2012).

Generally, all the modified methods are aimed at improving the concentration of the TFR. In this study, we apply the synchroextracting transform (SET) (Yu et al., 2017) in seismic TFA to show its potential in fluvial channel detection with the 3D seismic data. The SET is inspired by the FSST and ITFA theory (Stanković et al., 2014). It only extracts the information of the STFT result that is most related to the IF of a signal (Yu et al., 2017). Therefore, the SET can generate more sparse TFR compared with the FSST for time-varying signals. Even, we will give a theorem that the SET can provide a highly concentrated TFR for signals containing high FM modes, which is not considered by Yu et al. (2017). The more concentrated TFR denotes the better ability of the TF localization and the better characterization of time-varying features. So, we introduce the SET method for seismic data processing to enhance the quality of the TF result, and further improve the delineation of subsurface fluvial channels.

In this paper, we will show the desirable properties of the SET in the TFR of seismic signals. In the next section, we present the basic theoretical background concerning the STFT, FSST, and SET. We also give a theorem about the frequency estimation of a chirp signal to show that the SET still can obtain a highly concentrated TFR for the strongly FM signal. In a following section, several synthetic examples are employed to illustrate the performance in concentrating the TF distribution, and applications on field data further demonstrate the potential for subsurface channel characterizations. Finally, we draw conclusions in the last section.

THEORETICAL BACKGROUND

The short-time Fourier transform

The Fourier transform $\hat{f}(\eta)$ of the signal $f(t)\in L^1(R)$ is defined as the following normalization:

$$\hat{f}(\eta)=\int_{-\infty}^{+\infty} f(t)e^{-2i\pi\eta t}dt \quad . \tag{1}$$

As is well-known, the Fourier spectrogram $\hat{f}(\eta)$ only displays the frequency η of $f(t)$ on the whole time domain. To get the time-varying frequency spectrum, the short-time Fourier transform (STFT). For a given function $f(t)\in L^2(R)$ and a window function $g\in L^2(R)$, the STFT is defined by

$$V_f(\eta,t)=\int_{-\infty}^{+\infty} f(\xi)g(\xi-t)e^{-2i\pi\eta\tau}d\xi \quad , \tag{2}$$

which is a local version of the Fourier transform obtained by means of the sliding window $g\in L^2(R)$. Considering an additional phase shift $e^{2i\pi\eta t}$, the expression of the standard STFT can be modified as

$$V_f(\eta,t)=\int_{-\infty}^{+\infty} f(\xi)g(\xi-t)e^{-2i\pi\eta(\tau-t)}d\xi. \tag{3}$$

We now study the STFT of an amplitude-modulated and frequency-modulated (AM-FM) mode

$$f(t)=A(t)e^{2i\pi\phi(t)}, \tag{4}$$

where $A(t)$ and $\phi(t)$ are the time-varying amplitude and phase function of the signal $f(t)$, respectively. The derivative of the phase $\phi(t)$ is the instantaneous frequency (IF). If the amplitudes $A(t)$ and IF $\phi'(t)$ are positive and vary slowly enough, we can give a first-order expansion of the phase combined with a zero-th order expansion of the amplitude, which leads to the following approximation of $f(t)$

$$f(t)\approx A(t_0)e^{2i\pi[\phi(t_0)+\phi'(t-t_0)]}. \tag{5}$$

Then the corresponding approximation of the STFT is obtained as (Daubechies et al., 2011; Oberlin et al., 2014):

$$V_f(\eta,t)\approx f(t)\hat{g}(\eta-\phi'(t)), \tag{6}$$

which denotes that the spectrum energy of $f(t)$ is distributed along the *ridge* $\eta = \phi'(t)$ in the time-frequency (TF) plane. According to eq. (6), if the time-frequency representation (TFR) is concentrated enough, each signal $f(t)$ exists in a standalone TF strip [see Fig. 1(b)]. Then it allows for the detection and reconstruction. However, for the multicomponent signal, if the TF distribution $V_f(\eta,t)$ is not enough quality, the modes may overlap or couple in the TF plane [see Fig. 2(b)], which will affect the subsequent processing.

Fourier-based synchrosqueezing transform

The synchrosqueezing transform (SST) was originally proposed in the wavelet frame for the audio signal processing (Daubechies and Maes, 1996), and its corresponding theoretical analysis was provided by Daubechies et al. (2011) (Daubechies et al., 2011). The SST can sharpen the TFR of a signal using a nonlinear operator and allow for mode reconstruction. Like the SST, the aim of the Fourier-based synchrosqueezing transform (FSST) (Oberlin et al., 2014) is to provide a concentrated TFR that enables to detect and present the different modes within the signal. Analogously, the FSST reassigns the coefficients $V_f(\eta,t)$ according to the map (η,t) a $(\hat{\omega}_f(\eta,t),t)$ to enhance the concentration of the TFR obtained by the STFT. The frequency operator $\hat{\omega}_f(\eta,t)$ is the estimation of the local IF defined by (Auger and Flandrin, 1995)

$$\hat{\omega}_f(\eta,t) = \frac{1}{2\pi}\partial_t \arg V_f(\eta,t) = \Re\{\frac{1}{2i\pi}\frac{\partial_t V_f(\eta,t)}{V_f(\eta,t)}\}, \tag{7}$$

which is indeed a good local approximation of the IF $\phi'(t)$ for the weak AM-FM signal. Then, the FSST is expressed as

$$T_f(\omega,t) = \int_{-\infty}^{+\infty} V_f(\eta,t)\cdot\delta(\omega-\hat{\omega}_f(\eta,t))d\eta. \tag{8}$$

where δ is the Dirac distribution. Now, we show the performance of the FSST for the test signal in $f_1(t)$ Fig. 1. To obtain the IF estimation (7), we need to calculate the derivative of $V_f(\eta,t)$ with respect to time. According to eq. (6), we have

$$\begin{aligned}\partial_t V_f(\eta,t) &= \partial_t\{Ae^{2i\pi\omega_0 t}\cdot\hat{g}(\eta-\omega_0)\}\\ &= 2i\pi\cdot\omega_0\cdot V_f(\eta,t)\end{aligned}. \tag{9}$$

Then, submitting (9) into (7), we can get

$$\hat{\omega}_f(\eta,t) = \omega_0, \tag{10}$$

which means $\hat{\omega}_f(\eta,t)$ actually matching the IF ω_0 for the purely harmonic signal. In this case, the FSST achieves an ideal TFR [see Fig. 1(c)]. For the perturbations of pure waves that contains slowly-varying amplitude and instantaneous frequency. The correlative main theory analysis was given in (Behera et al., 2017), which provides a strong approximation result. The non-zero coefficients of the FSST result are localized on a TF strip centered on the instantaneous frequency $\phi'(t)$. To summarize, the FSST achieves a good localization if the following restrictive conditions are satisfied:

- the low-modulation assumption $\phi''(t) \le \varepsilon$.

Through the synchrosqueezing operation, the FSST obtains a significantly higher concentrated TFR than the modified STFT [see Fig. 1(c) and Fig. 2(c)]. In practice, signals always contain high-modulation components, which means that the $\phi''(t)$ is non-negligible. For such signals with fast varying frequency, the FSST still inevitably results in a diffused TF distribution as labeled in Fig. 2(c).

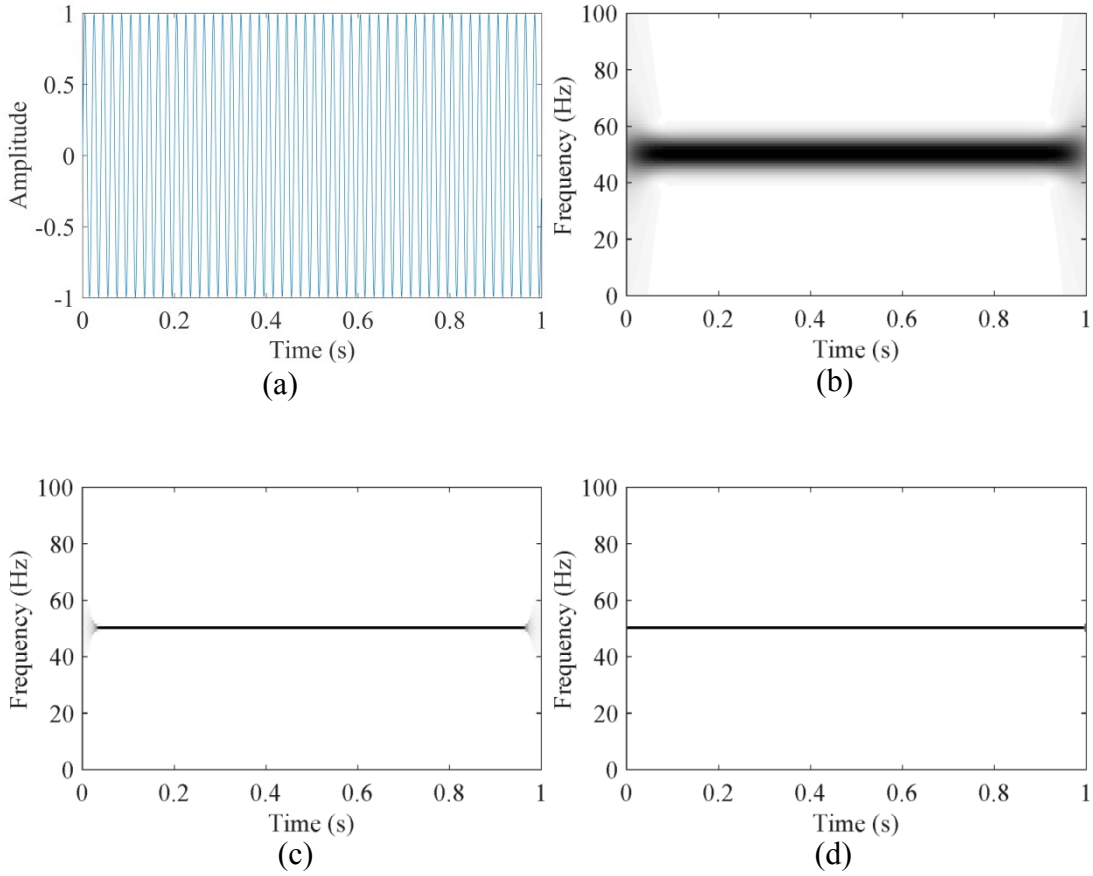

Fig. 1. The illustration of the harmonic signal $f_1(t)$. (a) The waveform, (b) the STFT result, (c) the FSST result, and (d) the SET result. Compared with the diffused TFR from the STFT, the FSST- or SET-based result provides a better one toward to the ideal TFR of $f_1(t)$.

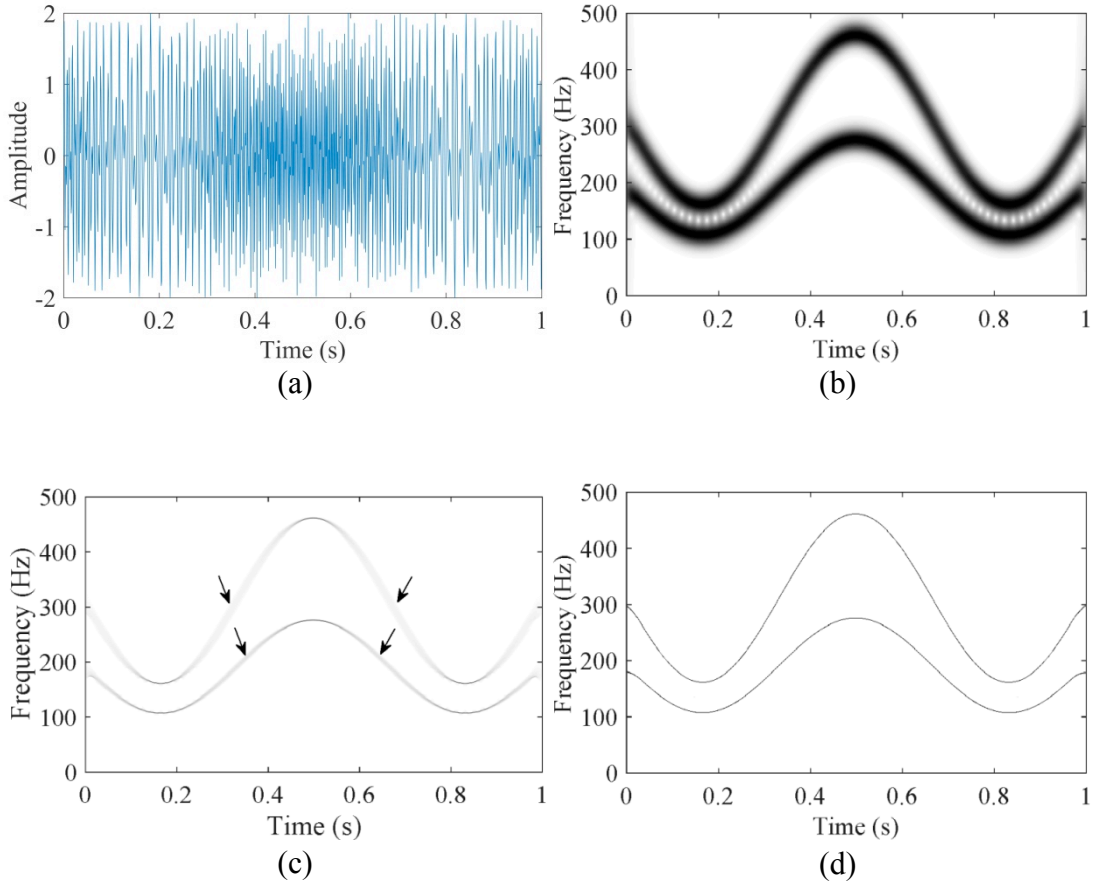

Fig. 2. The illustration of signal $f_2(t)$ with high FM modes. (a) The waveform, (b) the STFT result, (c) the FSST result, and (d) the SET result. The STFT- and FSST-based results are both diffused, while the SET provides a much concentrated TFR.

The synchroextracting transform

To further enhance the energy concentration of the TFR, Yu et al. (2017) proposed the synchroextracting transform (SET), which is different from the manner of the FSST. The definition of the SET is

$$Te(\eta,t) = V_f(\eta,t)\cdot\delta(\eta-\hat{\omega}_f(\eta,t)), \tag{11}$$

where δ is the discrete Delta function. The operator $\delta(\eta-\hat{\omega}_f(\eta,t))$ is defined by

$$\delta(\eta-\hat{\omega}_f(\eta,t)) = \begin{cases} 1 & \eta=\hat{\omega}_f(\eta,t) \\ 0 & \eta\neq\hat{\omega}_f(\eta,t). \end{cases} \tag{12}$$

Then, submitting this equation to (11), it holds

$$Te(\eta,t) = \begin{cases} V_f(\eta,t) & \eta=\hat{\omega}_f(\eta,t) \\ 0 & \eta\neq\hat{\omega}_f(\eta,t). \end{cases} \tag{13}$$

So, we can use the coefficients only in trajectory $\eta = \hat{\omega}_f(\eta,t)$ to sharp the TFR of the STFT. Due to the extracting manner (13), this novel method is termed SET, and $\delta(\eta - \hat{\omega}_f(\eta,t))$ denotes the synchroextracting operator (SEO).

By analyzing the steps of the FSST and SET, the only difference between them is the last process [i.e., eqs. (8) and (11)]. Starting from the STFT, the FSST squeezes the coefficients $V_f(\eta,t)$ into a more compact TF domain according to the map (η,t) a $(\hat{\omega}_f(\eta,t),t)$. While the SET only extracts the coefficients of $V_f(\eta,t)$ where $\eta = \hat{\omega}_f(\eta,t)$. Fig. 1(d) shows that the SET achieves a perfect result for the harmonic wave the same as that of FSST. Moreover, it gets a more concentrated TFR for the signal with strong FM modes, as displayed in Fig. 2(d). In order to better analyze the different performance of the FSST and SET, we put forward the following theorem.

Theorem 1.

Consider a Gaussian window function and a pure linear chirp signal $f(t) = Ae^{2i\pi\phi(t)}$, where $\phi(t)$ is a second-order polynomial and $A > 0$. Then, for the reassignment operators $\hat{\omega}_f(\eta,t)$ [defined as eq. (7)], it holds $\hat{\omega}_f(\eta,t) = \phi'(t) + \dfrac{(\phi''(t))^2}{(b/\pi)^2 + (\phi''(t))^2}(\eta - \phi'(t))$ and $\hat{\omega}_f(\phi'(t),t) = \phi'(t)$ at each time t.

The proof of this theorem is available in the Appendix.

Because $\dfrac{(\phi''(t))^2}{1/(\pi b)^2 + (\phi''(t))^2} < 1$, it holds $|\hat{\omega}_f(\eta,t) - \phi'(t)| \le |(\eta - \phi'(t))|$. Thus, the FSST indeed achieves a more energy-concentrated TFR compared with the STFT. Theorem 1 clearly proves that the frequency estimation $\hat{\omega}_f(\eta,t) \neq \phi'(t)$ as soon as $\phi''(t) \neq 0$ i.e. $c \neq 0$. If the $|\phi''(t)|$ is not small

enough, the deviation of the frequency estimation and the IF is non-negligible. This theorem also gives a theoretical analysis why the FSST obtains a diffused TFR for the high-modulation signals [see Fig. 2(c)], especially at parts indicated by the arrows. Furthermore, the bigger $|\phi''(t)|$ is, the more diffused the TFR (indicated by the arrows in Fig. 4). However, the SET can always extract an accurate IF even for the chirp signal. In this context, the SET provides a well-concentrated TFR for the signal containing high FM modes [see Fig. 2(d)]. The more concentrated TFR denotes a better ability of the TF localization and a better characterization of the time-varying features, which is useful for seismic signal processing.

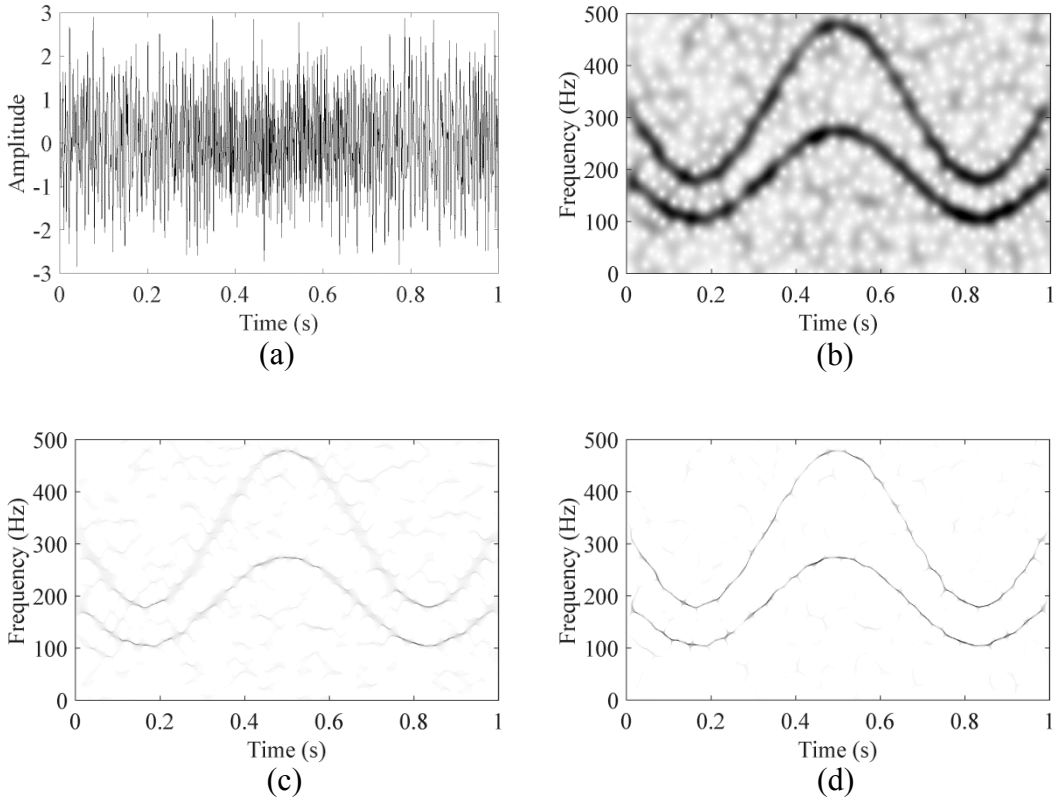

Fig. 3. Example of a noisy signal. (a) The noisy signal obtained by the signal $f_2(t)$ added with 5dB noise. The TF distributions achieved by the (b) STFT, (c) FSST, (d) SET.

NUMERICAL SIMULATIONS

Synthetic signals

In this section, we apply the proposed SET to three simulation data to illustrate its capability and effectiveness. The first simulated data is shown in Fig. 3(a), which is the signal $f_2(t)$ added with the Gaussian white noise. The signal-to-noise ratio (SNR) in Fig. 3(a) equals to 5 dB. The second one is a synthetic seismic trace containing three different seismic wavelets, as displayed in Fig. 4(a). Fig. 5(a) represents the last example, which comes from adding the 5dB Gaussian white noise to the second simulated signal in Fig. 4(a). Note that we introduce the STFT and FSST as the contrast methods.

The SET spectrum of the signal $f_2(t)$ has been shown in Fig. 2(d), which is more concentrated than the other two spectra in Figs. 2(b) and 2(c). In practice, the analyzed signal often contains noise which makes it difficult to achieve an uncontaminated TFR. The STFT is particularly sensitiveness to the Gaussian white noise, hence, its spectrum in Fig. 3(b) is blurred badly. Fig. 3(c) shows the TFR computed by the FSST with a better robustness than that calculated by the STFT. However, the energy still spreads out, especially where the frequency components change quickly. In Fig. 3(d), the SET spectrum is the most robustness and energy-concentrated. Thereby, images in Fig. 3 illustrate the robustness and effectiveness of the SET.

The second synthetic signal is a seismic trace in Fig. 4(a). It is composed of three seismic wavelets with different dominant frequencies. The dominant frequency of the first event is 30 Hz and the arrival time is 0.2 s. The second wavelet is a superposition of two Ricker wavelets with a 50 Hz domain frequency and arrive at 0.7 s and 0.715 s, respectively. The TFRs produced by the three methods are shown in Figs. 4(b), 4(c), and 4(d). The STFT obtains a fuzzy TFR [in Fig. 4(b)] and cannot describe the second event clearly and precisely. The FSST improves the readability of the TF distribution [in Fig. 4(c)] and is almost able to distinguish different wavelets at different time locations, but its spectrum is slightly fuzzy because of the energy diffusion. The SET result, as represented in Fig. 4(d), is the most concentrated and distinguishes the events the most clearly and accurately among these three spectra. Hence, we can easily draw a conclusion that the proposed SET based method can characterize subtle TF features of the analyzed signal by achieving a concentrated TF spectrum.

We add the Gaussian white noise to the synthetic seismic trace [in Fig. 4(a)] to verify the stability of the SET. Fig. 5(a) displays the noisy seismic trace, whose SNR is 5dB. The STFT and FSST are both blurred by the noise, and cannot characterize different wavelets well, shown in Figs. 9(b) and 9(c). The SET image shows the different wavelet clearly (indicated by the black arrows), and it is almost not affected by the added noise. Thus, the SET is more stable and more effective in the TF analysis of seismic signals compared with the STFT and FSST.

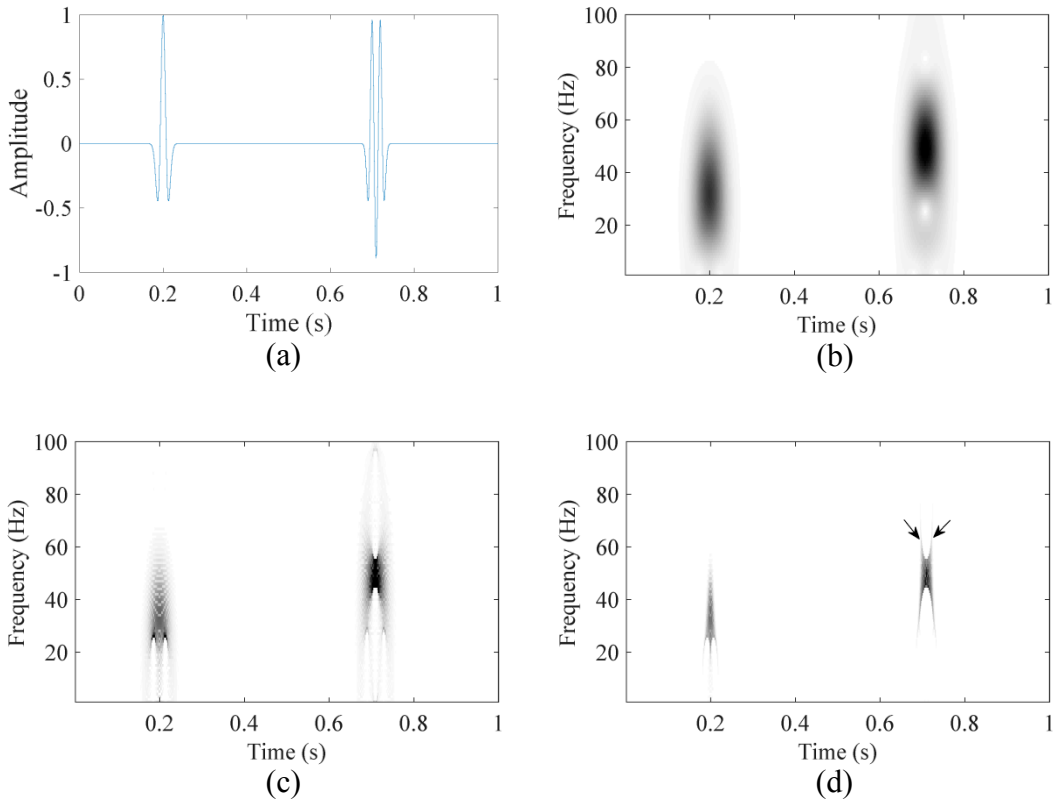

Fig. 4. The synthetic trace. (a) The single trace data. The TFR of the trace obtained by the (b) STFT, (c) FSST, and (d) SET.

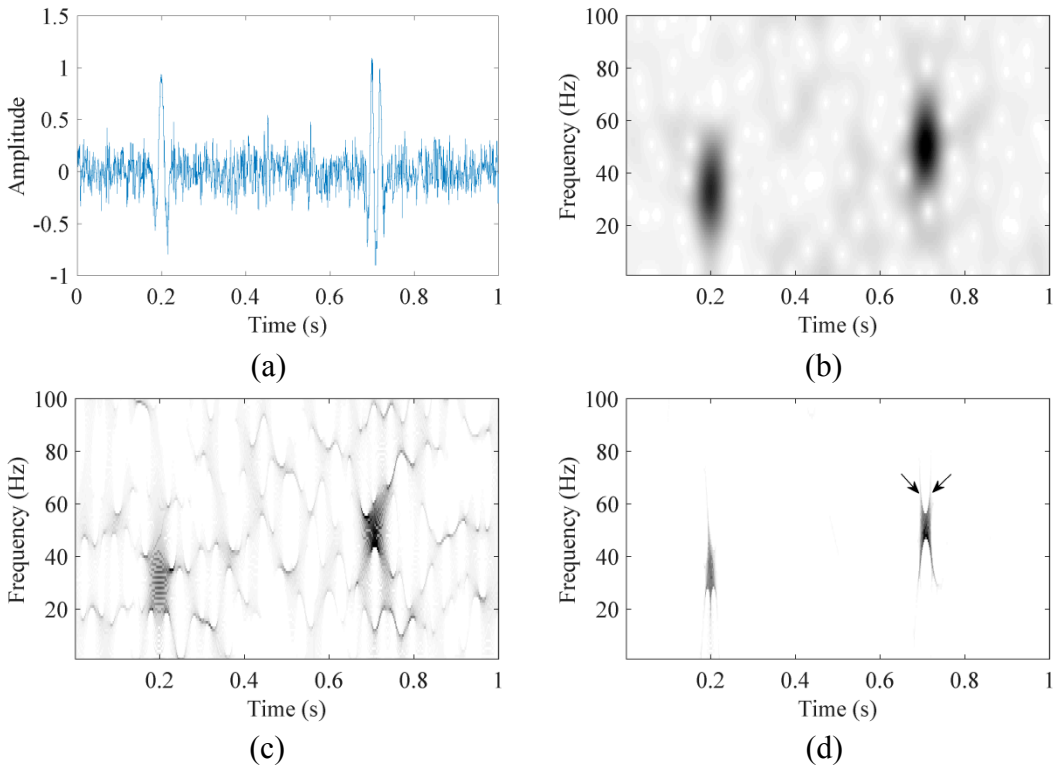

Fig. 5. The noisy synthetic trace. (a) The trace [in Fig. 8(a)] under 0 dB noise level. The TFR of the noisy trace calculated by the (b) STFT, (c) FSST, (d) SET.

Field data

To further prove the availability of the SET, we apply it to a 3D seismic data from a sedimentary basin in China. Both of the crossline and inline numbers are 401. The horizon slice of this 3D field data is shown in Fig. 6. Fig. As the study (Wang et al., 2012), the fluvial channels mainly controls the reservoir. There are many channel structures in this area, but they are distinguished difficultly. We can only see a few large-scale channels with discontinuity in the slice.

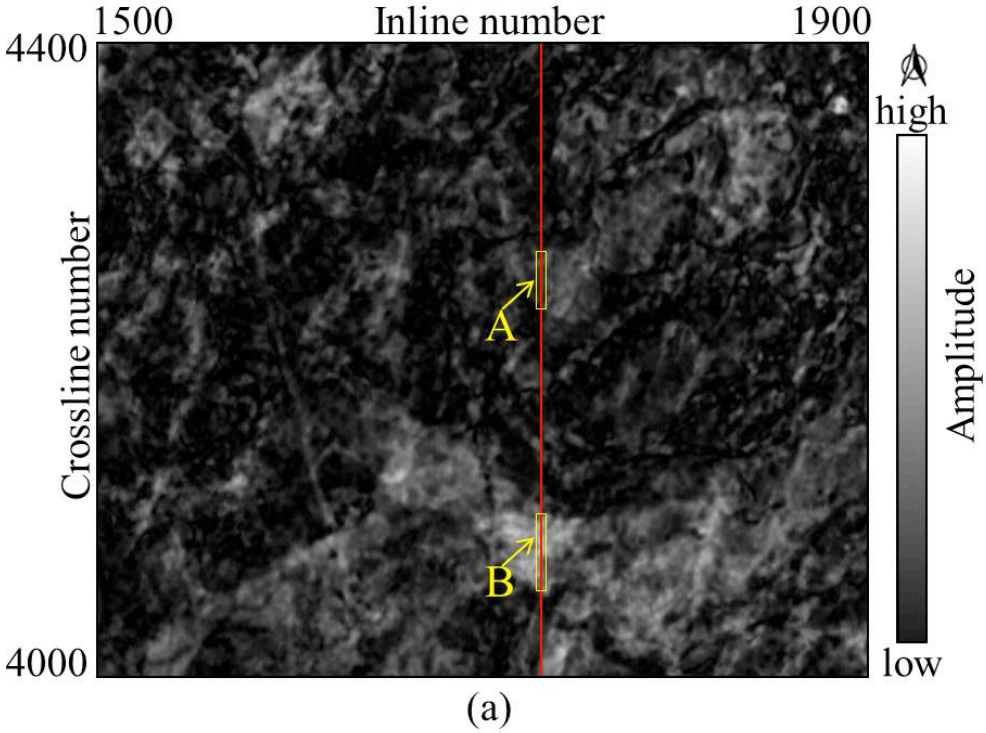

Fig. 6. A horizon slice of a 3D seismic data from a sedimentary basin in China. This 3D seismic volume, with 401 inlines and 401 crosslines, contains many flow channels.

Firstly, we process the seismic section of inline 1729, indicated the red line (in Fig. 6), that over the channels A and B. The corresponding section are displayed in Fig. 7. The two fluvial channels are generated at 1.22 s and 1.25 s, respectively. One is between common-midpoints (CMP) 4060 and 4120 (left ellipse), the other one is between CMP 4265 and 4305 (right ellipse). We extract the CMP 4285 that cross the channel A, as represented in Fig. 8(a). The corresponding TF image obtained by the STFT, FSST, and SET are shown in Figs. 8(b), 8(c) and 8(d), respectively. Due to the seismic attenuation, the frequency is damped with time increasing. In each time-frequency plane, there is a strong 30-Hz anomaly at 1.25 s because of the channel trace. Due to the energy diffusion, the results of the STFT [in Fig. 8(b)] and FSST [in Fig. 8(c)] are both blurry. The SET provides a more energy-concentrated TFR, so it displays the time and frequency locations of the anomaly clearly. Fig. 9 represents the 30-Hz sections of the STFT, FSST and SET results of the seismic section. Compared with the other two

methods, the SET provides a result with the higher TF resolution. Thus the SET presents the location and extent of spectral anomalies more accurately. In the spectrogram of the SET, the energy is sparser and more concentrated, which is more beneficial to further detect the edges of fluvial channels [see Fig. 9(c)].

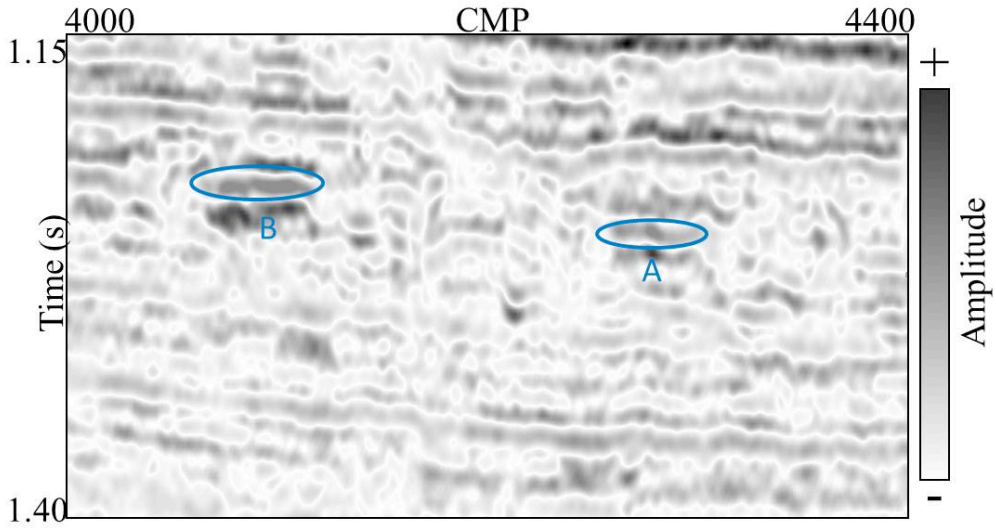

Fig. 7. The seismic section of inline 1729 over the channel A and B, as highlighted by the ellipses.

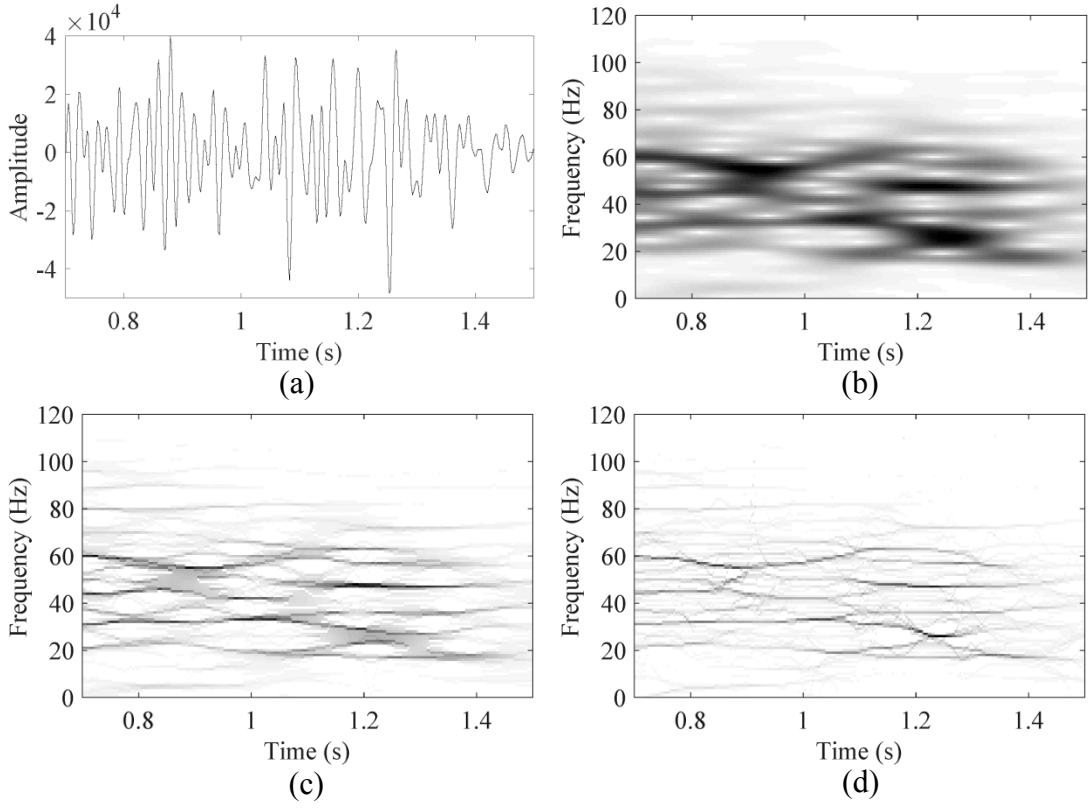

Fig. 8. (a) The CMP 4285 in Fig. 7. It crossed the channel at 1.25 s. The TFR of the CMP 180 gained by the (b) STFT, (c) FSST, (d) SET. The channel generates a strong 30-Hz anomaly at 1.25 s.

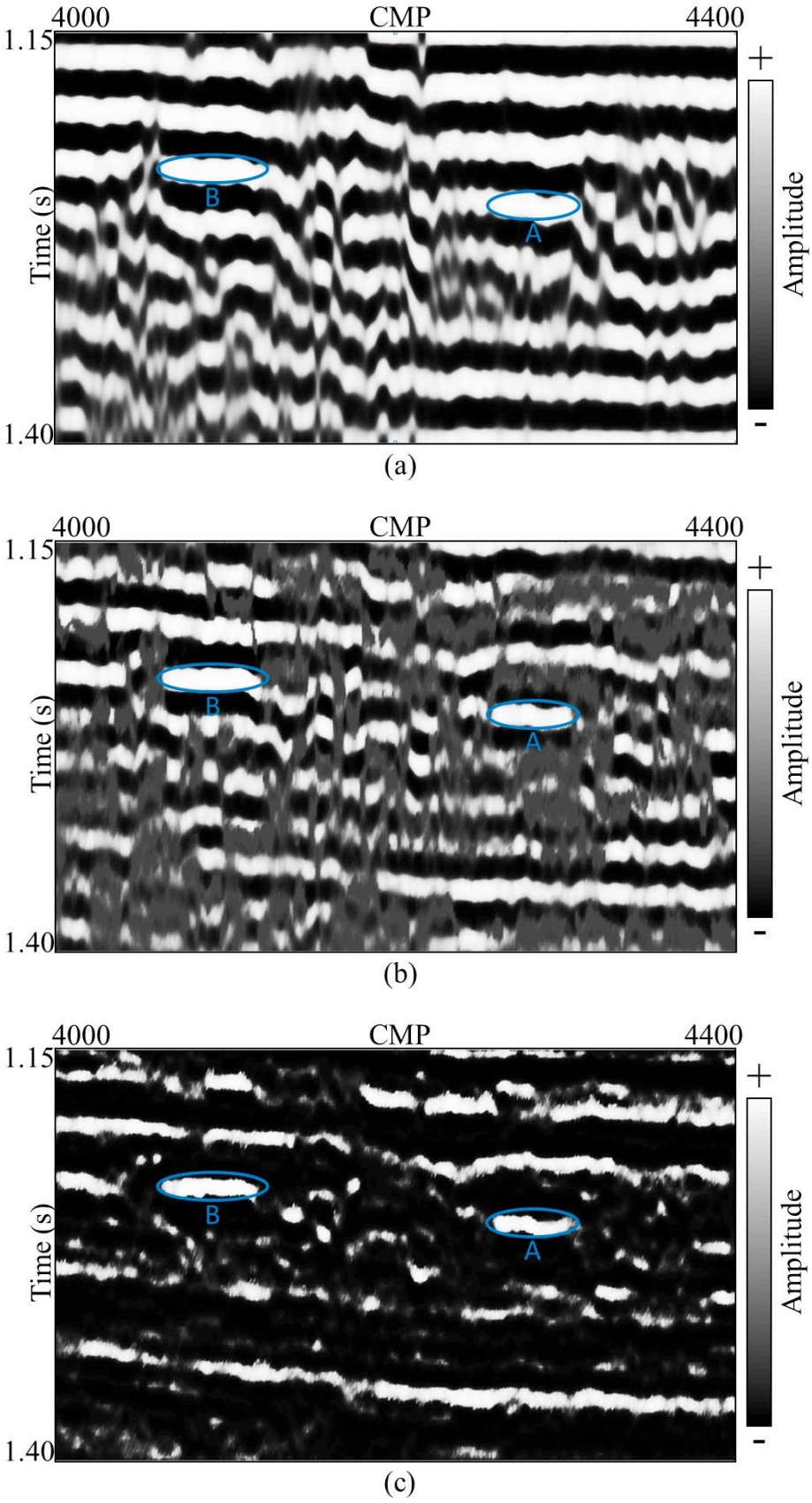

Fig. 9. The 30-Hz sections of the various TF spectrums using the (a) STFT, (b) FSST, and (c) SET. The SET obtains a higher time-frequency resolution and characterizes the fluvial channels more clearly.

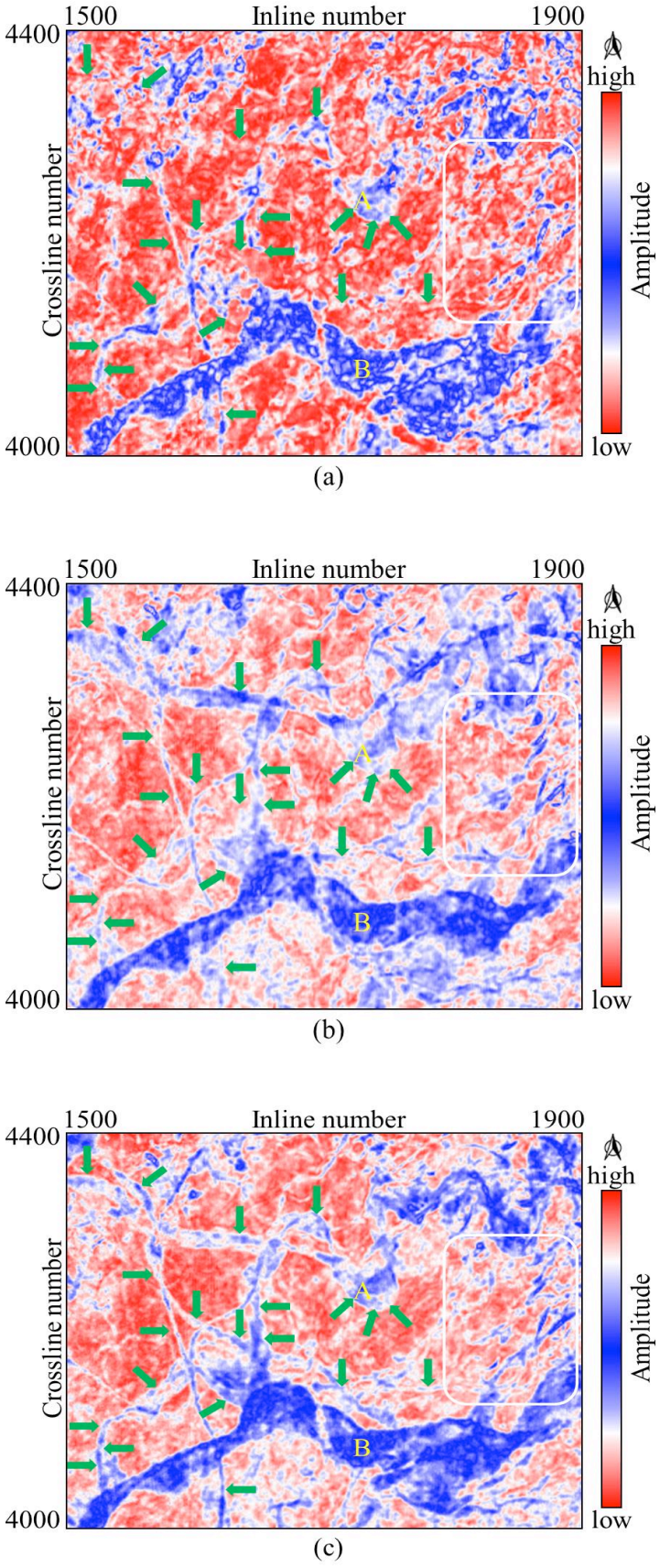

Fig. 10. The 50 Hz seismic slices of the 3D field seismic data from the various TFRs obtained by the (b) STFT, (c) FSST, and (d) SET. The channels are indicated by the green arrows and white ellipse.

Then, we employ the various TF algorithms to calculate the single frequency volume of the 3D seismic data in Fig. 6. As shown in Fig. 10, we extract the 30-Hz horizontal slices from the different TFRs in our work. The features of the STFT image [Fig. 10(a)] are obscure because of the diffused energy. As indicated by the green arrows and white ellipse, the FSST [Fig. 10(b)] and the SET [Fig. 10(c)] results display the potential fluvial channel more clearly. We also obtain that the results are consistent with the Fig. 9 at the channel A and B. Owing to the enhancement in the energy concentration and robustness, the SET image reveals more distinct and continuous subtle fluvial channels features, especially the boundaries of channels. To better compare the SET with the FSST, we introduce the red-green-blue (RGB) color-blending technique, which is applied to represent the 30-Hz, 45-Hz, and 60-Hz spectral components. The corresponding color-blending results are shown in Fig. 11. The RGB image describes more subsurface structures compared the single frequency slice, such those parts that are indicated by the yellow arrows and white ellipse in Fig. 10. Through the comparing, the SET describes the more continuous channels and clearer thicknesses of channel sand than the FSST, especially in the white ellipse. Thus, the seismic spectrum analysis with the SET is more helpful in indicating the geologic details.

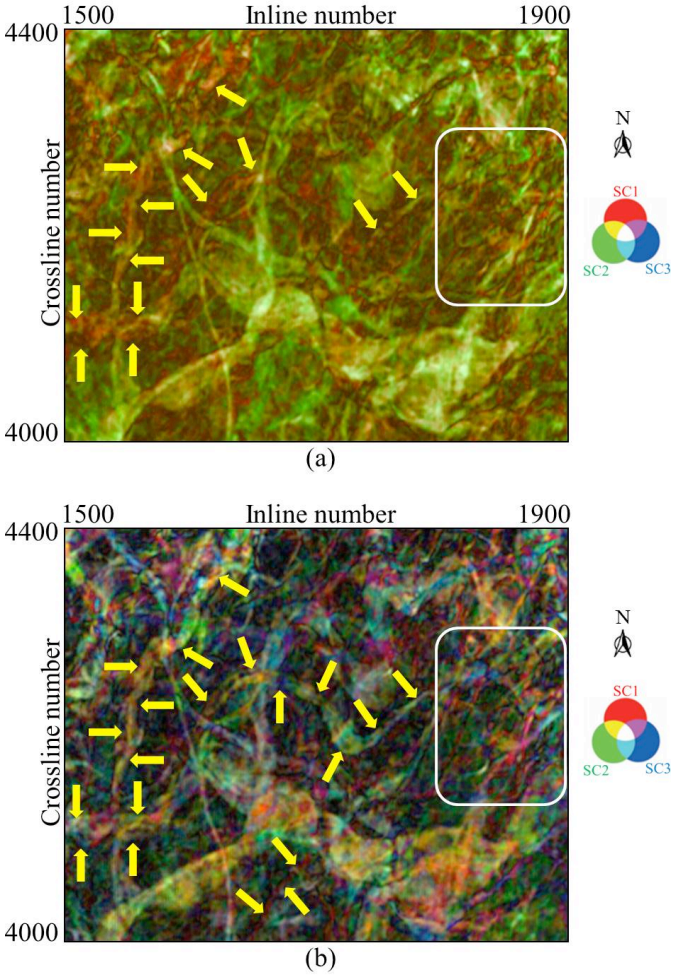

Fig. 11. The RGB blending results of the spectral components (SCs) at 30 Hz (red), 50 Hz (green), and 70 Hz (blue) obtained by the (a) FSST and (b) SET.

CONCLUSIONS

In this paper, we provided a theorem that the SET could achieve the exact IF for the chirp signal. Thus, the SET is suitable for processing the signal with highly FM modes. The experiments on the synthetic multicomponent signals show that the SET can achieve a TFR with better TF concentration compared with the STFT and FSST. The more energy-concentrated TF distribution leads to the better ability of the TF localization and the better characterization of the time-varying features in the TF plane. The improvement of the TF concentration makes the SET attractive in seismic data processing and interpretation for better describing subsurface geological structures. The SET-based results of the 2D and 3D data provide a better localization and delineate more details of fluvial channels, which demonstrates the potential of the SET for the seismic time-frequency analysis.

ACKNOWLEDGMENTS

This work is supported in part by the Major Research Plan of the National Natural Science Foundation of China (91730306), in part by the Major National Science and Technology Projects (2016ZX05024-001-007 and 2017ZX05069), and in part by the National Key R & D Project of the Ministry of Science and Technology of China (2018YFC0603501). The authors appreciate the editor and reviewers for their valuable comments, which improve the presentation of this work.

REFERENCES

Auger, F. and Flandrin, P., 1995. Improving the readability of time-frequency and time-scale representations by the reassignment method. IEEE Transact. Sign. Process., 43: 1068-1089.

Auger, F., Flandrin, P., Lin, Y., McLaughlin, S., Meignen, S., Oberlin, T. and Wu, H.T., 2013. Time-frequency reassignment and synchrosqueezing: An overview. IEEE Sign. Process. Mag., 30(6): 32-41.

Behera, B., Meignen, S. and Oberlin, T., 2018. Theoretical analysis of the second-order synchrosqueezing transform. Appl. Computat. Harmon. Analys., 45: 379-404.

Chen, Y., Liu, T., Chen, X., Li, J. and Wang, E., 2014. Time-frequency analysis of seismic data using synchrosqueezing wavelet transform. J. Seismic Explor., 23: 303-312.

Daubechies, I., 1992. Ten Lectures on Wavelets. SIAM, Philadelphia, PA, U.S.A.

Daubechies, I. and Maes, S., 1996. A nonlinear squeezing of the continuous wavelet transform based on auditory nerve models. Wavel. Medic. Biol., 30: 527-546.

Daubechies, I., Lu, J. and Wu, H.T., 2011. Synchrosqueezed wavelet transforms: An empirical mode decomposition-like tool. Appl. Comput. Harmon. Anal., 30: 243-261.

Gabor, D., 1946. Theory of communication. Part 1: The analysis of information. Radio Communicat. Engineer., 93: 429-441.

Gao, J., Chen, W., Li Y. and Tian, F., 2003. Generalized S-transform and seismic response analysis of thin interbeds. Chin. J. Geophys., 46: 526-532.

Gao, J., Wan, T., Chen, W. and Mao, J., 2006. Three parameter wavelet and its applications to seismic data processing:. Chin. J. Geophys., 49: 337-347.

Gao, J., Wang, W., Zhu, G., Peng, Y. and Wang, Y., 1996. On the choice of wavelet functions for seismic data processing. Chin. J. Geophys., 39: 392-400.

Hlawatsch, F. and Boudreaux-Bartels, G., 1992. Linear and quadratic time-frequency signal representations. IEEE Sign. Process. Magaz., 9(2): 21-67.

Herrera, R., Han, J. and van der Baan, M., 2014. Applications of the synchrosqueezing transform in seismic time-frequency analysis. Geophysics, 79(3): V55-V64.

Li, C. and Liang, M., 2012. A generalized synchrosqueezing transform for enhancing signal time–frequency representation. Sign. Process., 92: 2264-2274.

Li, F., Zhou, H., Zhao, T. and Marfurt, K.J., 2016. Unconventional reservoir characterization based on spectrally corrected seismic attenuation estimation. J. Seismic Explor., 25: 447-461.

Lilly, J. and Olhede, S.C., 2010. On the analytic wavelet transform. IEEE Transact. Informat. Theory, 57: 4135-4156.

Liu, J. and Marfurt, K.J., 2007. Instantaneous spectral attributes to detect channels. Geophysics, 72(2): P23-P31.

Liu, N., Gao, J. and Wang, Q., 2015. The extraction of instantaneous frequency from seismic data via synchrosqueezing three parameter wavelet transform. Expanded Abstr., 85th Ann. Internat. SEG Mtg., New Orleans: 2801-2805.

Liu, N., Gao, J., Zhang, B., Li, F. and Wang, Q., 2018. Time–frequency analysis of seismic data using a three parameters S-transform. IEEE Geosci. Remote Sens. Lett., 15: 142-146.

Liu, N., Gao, J., Zhang, Z., Jiang, X. and Lv, Q., 2017. High resolution characterization of geological structures using synchrosqueezing transform. Interpretation, 5: T75-T85.

Liu, W., Cao, S., Liu, Y. and Chen, Y., 2016. Synchrosqueezing transform and its applications in seismic data analysis. J. Seismic Explor., 25: 27-44.

Lu, W. and Zhang, Q., 2009. Deconvolutive short-time Fourier transform spectrogram. IEEE Sign. Process. Lett., 16: 576-579.

Lu, W. and Li, F., 2013. Seismic spectral decomposition using deconvolutive short-time Fourier transform spectrogram. Geophysics, 78(2): V43-V51.

Mallat, S.G. and Zhang, Z., 1993. Matching pursuits with timefrequency dictionaries. IEEE Transact. Sign. Process., 41: 3397-3415.

Mallat, S.G., 2008. A Wavelet Tour of Signal Processing: The Sparse Way. Academic Press, Orlando, FL.

Morlet, J., Arens, G., Fourgeau, E. and Glard, D., 1982, Wave propagation and sampling theory. Part I: Complex signal and scattering in multilayered media. Geophysics, 47: 203-221.

Oberlin, T., Meignen, S. and Perrier, V., 2014. The Fourier-based synchrosqueezing transform. IEEE Internat. Conf. Acoust., Speech Sign. Process. (ICASSP)}, 315-319.

Partyka, G. and Gridley, J., 1999. Interpretational applications of spectral decomposition in reservoir characterization. The Leading Edge, 18: 353-360.

Sejdić, E., Djurović, I. and Jiang, J., 2008. A window width optimized S-transform. EURASIP, J. Adv. Sign. Process.

Stanković, L., Djurović, I., Stanković, S., Simeunović, M., Djukanović, S. and Daković, M., 2014. Instantaneous frequency in time–frequency analysis: Enhanced concepts and performance of estimation algorithms. Digit. Sign. Process., 35: 1-13.

Stockwell, R., Mansinha, L. and Lowe, R., 1996. Localization of the complex spectrum: The S-transform. IEEE Transact. Sign. Process., 44: 998-1001.

Tary, J.B., Herrera, R.H., Han, J. and van der Baan, M., 2014. Spectral estimation-What is new? What is next?. Rev. Geophys., 52:723-749.

Wang, P., Gao, J. and Wang, Z., 2014. Time-frequency analysis of seismic data using synchrosqueezing transform. IEEE Geosci. Remote Sens. Lett., 11: 2042-2044.

Wang, Q., Gao, J., Liu, N. and Jiang, X., 2018. High resolution seismic time frequency analysis using the synchrosqueezing generalized S-transform. IEEE Geosci. Remote Sens. Lett., 15: 374-378.

Wang, Q. and Gao, J., 2017. Application of synchrosqueezed wave packet transform in high-resolution seismic time-frequency analysis. J. Seismic Explor., 26: 587-599.

Wang, X., Zhang, B., Li, F., Qi, J. and Bai, B., 2016. Seismic time-frequency decomposition by using a hybrid basismatching pursuit technique. Interpretation, 4(2): T263-T272.

Wang, Y., 2007. Multichannel matching pursuit for seismic trace decomposition. Geophysics, 75(4): V61-V66.

Wang, Z., Yin, C., Fan, T. and Lei, X., 2012. Seismic geomorphology of a channel reservoir in Lower Minghuazhen Formation, Laizhouwan subbasin, China. Geophysics, 77(4): B187-B195.

Yu, G., Yu, M. and Xu, C., 2017. Synchroextracting transform. IEEE Transact. Ind. Electron., 64: 8042-8054.

APPENDIX

We consider a linear chirp signal $f(t) = Ae^{2i\pi\phi(t)}$ with $\phi(t) = a_1 + b_1 t + \frac{1}{2}c_1 t^2$ and a generalized Gaussian window function $g(t) = ae^{-bt^2}$. For such a signal, wherever *t* and τ, we have

$$x(\tau + t) = x(t)e^{2i\pi[\phi'(t)\tau + \frac{1}{2}\phi''(t)\tau^2]} \tag{A-1}$$

According to eq. (3), the STFT of the mode $f(t)$ is then derived as

$$\begin{aligned} V_f(\eta, t) &= \int_{-\infty}^{+\infty} f(\xi)\cdot g(\xi - t)\cdot e^{-2i\pi\eta(\xi - t)} d\xi \\ &= \int_{-\infty}^{+\infty} f(\tau + t)\cdot g(\tau)\cdot e^{-2i\pi\eta\tau} d\tau \\ &= \int_{-\infty}^{+\infty} f(t)e^{2i\pi[\phi'(t)\tau + \frac{1}{2}\phi''(t)\tau^2]}\cdot ae^{-b\tau^2}\cdot e^{-2i\pi\eta\tau} d\tau \\ &= a\cdot f(t)\int_{-\infty}^{+\infty} e^{(i\pi\phi''(t) - b)\tau^2} e^{-2i\pi\tau(\eta - \phi'(t))} d\tau \end{aligned} \tag{A-2}$$

with $\tau = \xi - t$. We can denote $u = b - i\pi\phi''(t)$ and $v = 2\pi(\eta - \phi'(t))$, then

$$\begin{aligned} V_f(\eta, t) &= a\cdot f(t)\int_{-\infty}^{+\infty} e^{-u\eta^2} e^{-i\eta v} d\eta \\ &= a\cdot f(t)\int_{-\infty}^{+\infty} e^{-u(\eta + \frac{iv}{2u})^2} d\eta \cdot e^{-\frac{v^2}{4u}} \\ &= a\cdot f(t)\cdot\sqrt{\frac{\pi}{u}}\cdot e^{-\frac{v^2}{4u}} \end{aligned} . \tag{A-3}$$

Submitting u and v to (19), we obtain the final STFT result

$$V_f(\eta,t) = a \cdot f(t) \cdot \sqrt{\frac{\pi}{b - i\pi\phi''(t)}} \cdot e^{\frac{\pi^2(\eta-\phi'(t))^2}{b-i\pi\phi''(t)}} . \quad \text{(A-4)}$$

According to the formula (8) and $\phi'''(t) = 0$, we first calculate the derivative of

$$V_f(\eta,t)\ \partial_t V_f(\eta,t) = \phi'(t)V_f(\eta,t) + \frac{2(b + i\pi\phi''(t))(\phi''(t))^2}{(b/\pi)^2 + (\phi''(t))}(\eta - \phi'(t))V_f(\eta,t) \quad . \quad \text{(A-5)}$$

Then, we derive the expression of the IF estimation

$$\begin{aligned} \hat{\omega}_f(\eta,t) &= \Re\left(\frac{\partial_t V_f(\eta,t)}{2i\pi V_f(\eta,t)}\right) \\ &= \phi'(t) + \frac{(\phi''(t))^2}{(b/\pi)^2 + (\phi''(t))^2}(\eta - \phi'(t)) \end{aligned} . \quad \text{(A-6)}$$

It is easy to get the conclusion

$$\hat{\omega}_f(\phi'(t),t) = \phi'(t). \quad \text{(A-7)}$$